PDE Estimation Techniques for Advanced Battery Management Systems - Part I: SOC Estimation

S. J. Moura, N. A. Chaturvedi, and M. Krstić

***Abstract*— A critical enabling technology for electrified vehicles and renewable energy resources is battery energy storage. Advanced battery systems represent a promising technology for these applications, however their dynamics are governed by relatively complex electrochemical phenomena whose parameters degrade over time and vary across manufacturer. Moreover, limited sensing and actuation exists to monitor and control the internal state of these systems. As such, battery management systems require advanced identification, estimation, and control algorithms. In this paper we examine a new battery state-of-charge (SOC) estimation algorithm based upon the backstepping method for partial differential equations (PDEs). The estimator is synthesized from the so-called single particle model (SPM). Our development enables us to rigorously analyze observability and stability properties of the estimator design. In a companion paper we examine state-of-health (SOH) estimation, framed as a parameter identification problem for parabolic PDEs and nonlinearly parameterized output functions.**

I. INTRODUCTION

This paper investigates a Li-ion battery state-of-charge (SOC) estimation algorithm based upon the backstepping approach for partial differential equations (PDEs).

A. Motivation & Technical Challenges

Accurate battery SOC estimation algorithms are currently of extreme importance due to their applications in electrified transportation and energy storage systems for renewable sources. The relevancy of this topic is further underscored by the 27.2 billion USD federal government investment in energy efficiency and renewable energy research, including advanced batteries, under the American Recovery and Reinvestment Act (ARRA) of 2009. As such, battery management systems within these advanced transportation and energy infrastructures must have accurate knowledge of internal battery energy levels [1]. Such knowledge enables them to efficiently route energy while satisfying power demands and device-level operating constraints [2].

Monitoring battery SOC, which depends on the lithium concentration within each electrode, is particularly challenging for several technical reasons. First, directly measuring Li concentration is impractical outside specialized laboratory environments [3]. Second, the concentration dynamics are governed by partial differential algebraic equations derived from electrochemical principles [4], [5]. The only measurable quantities (voltage and current) are related to the states through nonlinear functions. Finally, the model parameters for these cells can vary widely with electrode chemistry, packaging, and time. In this paper we directly address the first two technical challenges. Namely, we design a state observer using a reduced-form PDE model based upon electrochemical principles. The measurements depend on the boundary states through a static nonlinear mapping. The companion paper addresses the third challenge as a parameter identification problem.

This work was supported by the University of California Presidential Postdoctoral Fellowship Program and the National Science Foundation.

S. J. Moura and M. Krstic are with the Department of Mechanical and Aerospace Engineering and Cymer Center for Control Systems and Dynamics at the University of California, San Diego, CA 92093-0411, USA (e-mail: smoura@ucsd.edu; krstic@ucsd.edu)

N. A. Chaturvedi is with Robert Bosch LLC, Research & Technology Center, Palo Alto, CA 94304 USA (e-mail: nalin.chaturvedi@us.bosch.com)

B. Literature Review

Over the past decade research on battery SOC estimation has experienced considerable growth. One may divide this research by the battery models each algorithm employs.

The first category considers estimators based upon equivalent circuit models (ECMs). These models use circuit elements to mimic the phenomenological behavior of batteries. For example, Plett applies extended Kalman filters [6] and sigma-point Kalman filters [7] to simultaneously identify the states and parameters of an ECM. Verbrugge and his co-workers used ECMs with combined coulumb-counting and voltage inversion techniques in [8] and adaptive parameter identification algorithms in [9]. A similar approach in [10] uses an indirect nonlinear adaptive observer. Impedance-based ECMs, as opposed to voltage-based ECMS, were applied to the SOC estimation problem in [11]. The key advantage of ECMs is their simplicity. However, they often require extensive parameterization for accurate predictions. This often produces models with non-physical parameters whose complexity becomes comparable to electrochemical models.

The second category considers electrochemical models, which account for the diffusion, intercalation, and electrical dynamics. Although these models can accurately predict internal state variables, their mathematical structure is often too complex for controller/observer design. Therefore, these approaches combine model reduction and estimation techniques. One of the first studies within this category uses a "single particle model" (SPM) of electrochemical battery dynamics in combination with an extended Kalman filter [12]. Later, these authors added electrolyte dynamics to this model and applied an unscented Kalman filter [13]. A variation of the SPM, known as electrode average model, was developed in [14] in conjunction with an extended Kalman filter. A

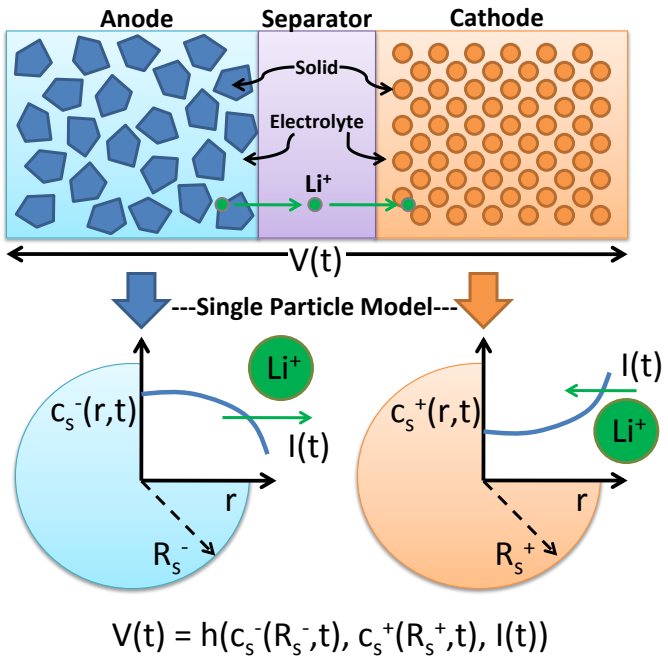

Fig. 1. Schematic of single particle model of a Li-ion battery. Each electrode is idealized as a single porous spherical particle. During charging and discharging Li intercalates into/out of these spherical particles. The diagram depicts several important model variables, including input current $I(t)$, terminal voltage $V(t)$, and Li concentration distributions in the anode $c_s^-(r,t)$ and cathode $c_s^+(r,t)$.

separate research group employed residue grouping for model reduction and linear Kalman filters for observers [15] and constraint governors [16]. Ultimately, all of these studies discretize the governing PDEs into a system of ODEs. In contrast, the authors of [17] develop a PDE-based observer. However the stability properties of this design remains as an open question due to the model complexity.

C. Contributions

In this paper we extend the aforementioned research in the following three ways. First, we rigorously analyze the observability properties of the SPM. This analysis leads us towards a single electrode SPM whose states are locally observable. Second, we design a PDE-based observer via the backstepping method. The resulting observer gains are related to a Klein-Gordon equation, which turns out to have a closed-form solution. The resulting gains are characterized by explicit closed-form expressions which do not require additional states, an added computational benefit. This is the first known application of PDE backstepping to the battery SOC estimation problem. Third, stability results for the estimation error dynamics are automatically generated through the backstepping design. That is, this method derives the output injection gains such that the estimation error dynamics match an exponentially stable target system.

D. Paper Organization

The paper is organized as follows: Section II describes the electrochemical-based single particle model and its observability properties. Section III develops a backstepping PDE observer for a reduced form version of the SPM and evaluates its performance via simulation studies. Finally, Section IV concludes the paper by summarizing its main results.

TABLE I
SINGLE PARTICLE MODEL PARAMETER DEFINITIONS

Symbol	Description	SI Units
A	Cell cross sectional area	m^2
a^j	Specific interfacial surface area	m^2/m^3
c_e^0	Li concentration in electrolyte phase	mol/m^3
c_s^j	Li concentration in solid phase	mol/m^3
c_{ss}^j	Li concentration at particle surface	mol/m^3
$c_{s,max}^j$	Max Li concentration in solid phase	mol/m^3
D_s^j	Diffusion coefficent in solid phase	m^2/sec^3
F	Faraday's constant	C/mol
I	Input current	A
i_0^j	Exchange current density	V
j	Positive (+) or negative (-) electrode	-
k^j	Reaction rate	$A{\cdot}mol^{1.5}/m^{5.5}$
L^j	Electrode thickness	m
R	Universal gas constant	J/mol-K
R_f	Lumped current collector resistance	Ω
R_s^j	Particle radius	m
r	Radial coordinate	m or m/m
T	Cell temperature	K
t	Time	sec or sec/sec
U^j	Equilibrium potential	V
V	Output voltage	V
α^j	Anodic/cathodic transfer coefficient	-
ϵ_s^j	Volume fraction of solid phase	-

II. SINGLE PARTICLE MODEL & ANALYSIS

The single particle model (SPM) was first applied to lithium battery systems in [18] and is the model we utilize in this work. The key assumption is that the solid phase of each electrode can be idealized as a single spherical particle. In addition, the electrolyte concentration diffusion and migration dynamics are neglected and thermal effects are ignored. Figure 1 provides a schematic of the SPM concept. Mathematically, the model consists of two diffusion PDEs governing each electrode's concentration dynamics, where input current enters as a Neumann boundary condition. Output voltage is given by a nonlinear function of the state values at the boundary and the input current. Table I provides definitions for the parameters in the equations that follow.

Although this model arguably captures less dynamic behavior than other electrochemical-based estimation models [18], it has a sufficiently simple structure to make statements about observability - a unique point of this work.

A. SPM Development

Diffusion in each electrode is governed by Fick's law in spherical coordinates:

$$\frac{\partial c_s^-}{\partial t}(r,t) = D_s^- \left[\frac{2}{r}\frac{\partial c_s^-}{\partial r}(r,t) + \frac{\partial^2 c_s^-}{\partial r^2}(r,t)\right] \quad (1)$$

$$\frac{\partial c_s^+}{\partial t}(r,t) = D_s^+ \left[\frac{2}{r}\frac{\partial c_s^+}{\partial r}(r,t) + \frac{\partial^2 c_s^+}{\partial r^2}(r,t)\right] \quad (2)$$

with Neumann boundary conditions:

$$\frac{\partial c_s^-}{\partial r}(0,t) = 0, \quad \frac{\partial c_s^-}{\partial r}(R_s^-,t) = -\frac{I(t)}{D_s^- F a^- A L^-} \quad (3)$$

$$\frac{\partial c_s^+}{\partial r}(0,t) = 0, \quad \frac{\partial c_s^+}{\partial r}(R_s^+,t) = \frac{I(t)}{D_s^+ F a^+ A L^+} \quad (4)$$

The Neumann boundary conditions at $r = R_s^+$ and $r = R_s^-$ signify that the flux entering the electrode is proportional to the input current $I(t)$. The Neumann boundary conditions at $r = 0$ are required for well-posedness. Note that the states for the two PDEs are dynamically uncoupled, although they have proportional boundary inputs.

The measured terminal voltage output is governed by a combination of electric overpotential, electrode thermodynamics, and Butler-Volmer kinetics. The end result is:

$$\begin{aligned} V(t) = & \frac{RT}{\alpha^+ F}\sinh^{-1}\left(\frac{I(t)}{2a^+AL^+i_0^+(c_{ss}^+(t))}\right) \\ & -\frac{RT}{\alpha^- F}\sinh^{-1}\left(\frac{I(t)}{2a^-AL^-i_0^-(c_{ss}^-(t))}\right) \\ & +U^+(c_{ss}^+(t)) - U^-(c_{ss}^-(t)) - R_f I(t) \end{aligned} \quad (5)$$

where the exchange current density i_0^j and solid-electrolyte surface concentration c_{ss}^j are, respectively:

$$i_0^j(c_{ss}^j) = k^j\sqrt{c_e^0 c_{ss}^j(t)(c_{s,\max}^j - c_{ss}^j(t))} \quad (6)$$

$$c_{ss}^j(t) = c_s^j(R_s^j,t), \quad \mathrm{j} \in \{+,-\} \quad (7)$$

The functions $U^+(\cdot)$ and $U^-(\cdot)$ are the equilibrium potentials of each electrode material, given the surface concentration. Mathematically, these are strictly monotonically decreasing functions of their input. This fact implies that the inverse of its derivative is always finite, a property which we require later. Further details on the electrochemical principles used to derive these equations can be found in [1], [19].

This model contains the property that the total number of lithium ions is conserved [17]. Mathematically, $\frac{d}{dt}(n_{Li}) = 0$

$$\begin{aligned} n_{Li} = & \frac{\epsilon_s^+ L^+ A}{\frac{4}{3}\pi(R_s^+)^3}\int_0^{R_s^+} 4\pi r^2 c_s^+(r,t)dr \\ & + \frac{\epsilon_s^- L^- A}{\frac{4}{3}\pi(R_s^-)^3}\int_0^{R_s^-} 4\pi r^2 c_s^-(r,t)dr \end{aligned} \quad (8)$$

This property will become important, as it relates the total concentration of lithium in the cathode and anode. We leverage this fact to perform model reduction in the subsequent section.

B. Model Reduction & Observability

For the purpose of observer design we reduce the SPM by approximating the cathode diffusion dynamics (2) by its equilibrium. This step is mathematically motivated by the fact that the SPM states are weakly observable from voltage measurements, as has been previously noted in the literature [14]. It turns out that approximating the cathode as instantaneous produces a reduced system whose states are locally strongly observable. Moreover, physical motivation exists for this reduction when diffusion dynamics are significantly faster in the cathode than the anode, a common characteristic of certain anode/cathode combinations. We discuss these points in succession.

Lack of observability can be shown using a number of techniques. For example, one may (i) approximate the PDEs by ODEs using the finite difference method, producing a tri-diagonal matrix A, (ii) linearize the output equation about the states, producing a matrix C, (iii) and compute the rank of the observability matrix for the pair (A, C) [20].

The reduced SPM has a PDE given by (1), boundary conditions given by (3), and output equation:

$$\begin{aligned} V(t) = & \frac{RT}{\alpha^+ F}\sinh^{-1}\left(\frac{I(t)}{2a^+AL^+i_0^+(\alpha c_{ss}^-(t)+\beta)}\right) \\ & -\frac{RT}{\alpha^- F}\sinh^{-1}\left(\frac{I(t)}{2a^-AL^-i_0^-(c_{ss}^-(t))}\right) \\ & +U^+(\alpha c_{ss}^-(t)+\beta) - U^-(c_{ss}^-(t)) - R_f I(t) \end{aligned} \quad (9)$$

Note that $c_{ss}^+(t)$ has been replaced by $\alpha c_{ss}^-(t) + \beta$. This is the critical detail of the reduced SPM. The equilibrium of the cathode states (i.e., $c_s^+(r,t) = c_{ss}^+(t)$) can be computed from the conservation of Li property in (8) to produce the relationship[1]:

$$c_{ss}^+(t) = \frac{1}{\epsilon_s^+ L^+ A}\left[n_{Li} - \epsilon_s^- L^- A c_{ss}^-(t)\right] \quad (10)$$

where $\alpha = -\frac{\epsilon_s^- L^-}{\epsilon_s^+ L^+}$ and $\beta = \frac{n_{Li}}{\epsilon_s^+ L^+ A}$.

One can show this system is locally observable (i.e. in the linear sense) by using the same finite difference and linearization approach described above. Ultimately, we guarantee observability for this reduced SPM by designing the observer gains such that the estimation error dynamics mimic an exponentially stable target system. This is the core concept behind backstepping observer design [21].

Physical motivation also exists for approximating the cathode diffusion dynamics as instantaneous. Significant research efforts on manufacturing and material science techniques for cathode materials has enabled researchers to attain nano-scale particle sizes and faster diffusion rates [22]. The result is characteristic diffusion times (mathematically R_s^2/D_s) which are often orders of magnitude less in the cathode than the anode. Parallel studies have been performed on the anode side (see e.g. [23]), however they are less prevalent. Hence, approximating cathode diffusion its equilibrium is a reasonable approximation for certain cathode/anode combinations. This insight was also observed through a previous parameter identification study on commercially available $LiFePO_4$ cells with doped nano-scale cathode materials [24].

C. Existence of Nonlinear Output Function Inverse

Note that the SPM contains linear dynamics and a nonlinear output function. In general an output injection-based estimator

[1]To be technically correct, the cathode concentration should depend on the anode concentration summed over the spherical volume: $c_{ss}^+(t) = \frac{1}{\epsilon_s^+ L^+ A}\left[n_{Li} - \frac{3\epsilon_s^- L^- A}{4\pi R_s^{-3}}\int_0^{R_s^-} 4\pi r^2 c_s^-(r,t)dr\right]$. However, this results in a nonlinear output equation which depends on the *in-domain states*, as well as the boundary state. This would create additional complexity to the backstepping approach we employ in this paper.

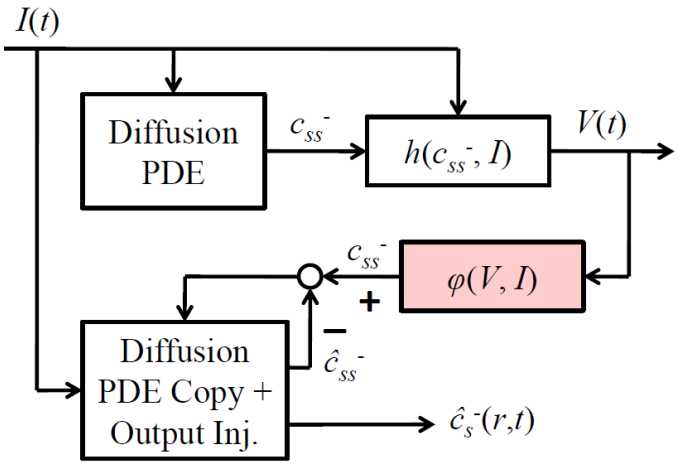

Fig. 2. Block diagram of estimation scheme where the *boundary state error* is injected into the estimator. The true boundary state c_{ss}^- is determined by $\varphi(V, I)$, which inverts the nonlinear output function w.r.t. the state, uniformly in the input current (highlighted in pink).

would be nonlinear for this class of systems. However, we design a *linear* estimator in this paper by *injecting the boundary state error*. This idea requires us to calculate the boundary state from the measured voltage, demonstrated visually by the block diagram in Fig. 2. That is, we must show the output function (9) is invertible with respect to the boundary state c_{ss}^-, uniformly in the input current $I(t)$.

Specifically, let $h : \mathbb{R} \times \mathbb{R} \to \mathbb{R}$ be defined such that $V(t) = h(c_{ss}^-(t), I(t))$. Then we must show h is a one-to-one function w.r.t. its first argument, uniformly in the second argument. The horizontal line test can be used to validate this claim. As a result, it is possible to determine the inverse function φ where $c_{ss}^-(t) = \varphi(V(t), I(t))$.

III. BACKSTEPPING OBSERVER DESIGN

A. Normalization, State Transformation, and Structure

In this subsection we perform normalization and state transformation to simplify the mathematical structure of the observer.

1) Normalization: First we scale the radial r and time t coordinates as follows:

$$\bar{r} = \frac{r}{R_s^-} \qquad \bar{t} = \frac{D_s^-}{(R_s^-)^2} t \tag{11}$$

which results in the following PDE and boundary conditions:

$$\frac{\partial c_s^-}{\partial \bar{t}}(\bar{r}, \bar{t}) = \frac{2}{\bar{r}} \frac{\partial c_s^-}{\partial \bar{r}}(\bar{r}, \bar{t}) + \frac{\partial^2 c_s^-}{\partial \bar{r}^2}(\bar{r}, \bar{t}) \tag{12}$$

$$\frac{\partial c_s^-}{\partial \bar{r}}(0, \bar{t}) = 0, \quad \frac{\partial c_s^-}{\partial \bar{r}}(1, \bar{t}) = -\frac{R_s^- I(\bar{t})}{D_s^- Fa^- AL^-} \tag{13}$$

Henceforth we will drop the bars over the space and time coordinates to simplify notation.

2) State Transformation: Next we perform a state transformation to eliminate the first spatial derivative in the spherical diffusion equation (12). Namely, let

$$c(r, t) = r c_s^-(r, t) \tag{14}$$

thus producing the following PDE plant:

$$\frac{\partial c}{\partial t}(r, t) = \frac{\partial^2 c}{\partial r^2}(r, t) \tag{15}$$

with Dirichlet and Robin boundary conditions:

$$c(0, t) = 0 \tag{16}$$

$$\frac{\partial c}{\partial r}(1, t) - c(1, t) = -\frac{R_s^-}{D_s^- Fa^- AL^-} I(t) \tag{17}$$

and nonlinear output map given by (9) where $c_{ss}^+ = \alpha\ R_s^- c(1, t) + \beta$ (see (10)) and $c_{ss}^- = c(1, t)$.

The transformation is invertible since

$$c_s^-(0, t) = \lim_{r \to 0} \frac{c(r, t)}{r} = \frac{\partial c}{\partial r}(0, t) \in \mathcal{L}_\infty \tag{18}$$

Therefore any stability properties established for the c-system also apply to the c_s^--system.

3) Observer Structure: The observer structure consists of a copy of the plant (15)-(17) plus *boundary state error injection*, as follows:

$$\frac{\partial \hat{c}}{\partial t}(r, t) = \frac{\partial^2 \hat{c}}{\partial r^2}(r, t) + p_1(r)\tilde{c}(1, t) \tag{19}$$

$$\hat{c}(0, t) = 0 \tag{20}$$

$$\frac{\partial \hat{c}}{\partial r}(1, t) - \hat{c}(1, t) = -\frac{R_s^- I(t)}{D_s^- Fa^- AL^-} + p_{10}\tilde{c}(1, t) \tag{21}$$

where the boundary state error is given by:

$$\tilde{c}(1, t) = \varphi(V(t), I(t)) - \hat{c}(1, t) \tag{22}$$

Note that the observer is *linear* because we use the boundary state for error injection. The plant boundary state is computed by inverting the nonlinear output mapping w.r.t. the boundary state, given a current input (i.e. $\varphi(V(t), I(t))$). Our next goal is to design the output injection gains $p_1(r)$ and p_{10} such that the state estimate converges exponentially to the true state.

B. Derivation of Output Injection Gains

The backstepping approach [21] is applied to design the output injection gains $p_1(r)$ and p_{10}. First, denote the observer error as $\tilde{c}(r, t) = c(r, t) - \hat{c}(r, t)$. Subtracting (19)-(21) from (15)-(17) produces the estimation error dynamics:

$$\frac{\partial \tilde{c}}{\partial t}(r, t) = \frac{\partial^2 \tilde{c}}{\partial r^2}(r, t) - p_1(r)\tilde{c}(1, t) \tag{23}$$

$$\tilde{c}(0, t) = 0 \tag{24}$$

$$\frac{\partial \tilde{c}}{\partial r}(1, t) - \tilde{c}(1, t) = -p_{10}\tilde{c}(1, t) \tag{25}$$

The backstepping approach seeks to find the upper-triangular transformation

$$\tilde{c}(r, t) = \tilde{w}(r, t) - \int_r^1 p(r, s)\tilde{w}(s) ds \tag{26}$$

which satisfies the exponentially stable target system:

$$\frac{\partial \tilde{w}}{\partial t}(r,t) = \frac{\partial^2 \tilde{w}}{\partial r^2}(r,t) + \lambda \tilde{w}(r,t) \quad (27)$$

$$\tilde{w}(0,t) = 0 \quad (28)$$

$$\frac{\partial \tilde{w}}{\partial r}(1,t) = -\frac{1}{2}\tilde{w}(1,t) \quad (29)$$

where $\lambda < 1/4$. The symbol λ is a design parameter that enables us to adjust the pole placement of the observer. The coefficient $-1/2$ in (29) ensures the target system is exponentially stable, as can be seen by the derivation below.

One can show that (27)-(29) is exponentially stable in the spatial L_2 norm by considering the Lyapunov function:

$$V_{\text{lyap}}(t) = \frac{1}{2}\int_0^1 \tilde{w}^2(r,t)dr \quad (30)$$

Taking the total time derivative and applying integration by parts yields:

$$\dot{V}_{\text{lyap}}(t) = -\frac{1}{2}\tilde{w}^2(1) - \int_0^1 \tilde{w}_r^2 dr + \lambda \int_0^1 \tilde{w}^2 dr \quad (31)$$

Recalling the Poincaré inequality

$$-\int_0^1 \tilde{w}_r^2 dr \leq \frac{1}{2}\tilde{w}^2(1) - \frac{1}{4}\int_0^1 \tilde{w}^2 dr \quad (32)$$

produces

$$\dot{V}_{\text{lyap}}(t) \leq -\left(\frac{1}{4} - \lambda\right)\int_0^1 \tilde{w}^2 dr = -\left(\frac{1}{2} - 2\lambda\right) V_{\text{lyap}}(t) \quad (33)$$

which by the comparison principle [25] implies $V_{\text{lyap}}(t) \leq V_{\text{lyap}}(0)\exp\left[-(1/2 - 2\lambda)t\right]$ or $\|\tilde{w}(t)\| \leq \|\tilde{w}(0)\|\exp\left[-(1/4 - \lambda)t\right]$. Hence the target system is exponentially stable for $\lambda < 1/4$.

Following the procedure outlined in [21], we find that the kernel $p(r,s)$ in (26) must satisfy the following conditions:

$$p_{rr}(r,s) - p_{ss}(r,s) = \lambda p(r,s) \quad (34)$$

$$p(0,s) = 0 \quad (35)$$

$$p(r,r) = \frac{\lambda}{2}r \quad (36)$$

defined on the domain $\mathcal{D} = \{(r,s)|0 \leq r \leq s \leq 1\}$. The output injection gains are:

$$p_1(r) = -p_s(r,1) - \frac{1}{2}p(r,1) \quad (37)$$

$$p_{10} = \frac{3-\lambda}{2} \quad (38)$$

These conditions compose a Klein-Gordon PDE, which coincidentally has an analytic solution, discussed next.

C. Analytic Solution to Kernel PDE

The Klein-Gordon PDE in (34)-(36) has the closed form solution:

$$p(r,s) = \lambda r \frac{I_1(\sqrt{\lambda(r^2 - s^2)})}{\sqrt{\lambda(r^2 - s^2)}} \quad (39)$$

which can be solved by converting the PDE into an equivalent integral equation and applying the method of successive approximations [21]. Ultimately, this closed form solution provides the following output injection gains:

$$p_1(r) = \frac{-\lambda r}{2x}\left[I_1(x) - \frac{2\lambda}{x}I_2(x)\right] \quad (40)$$

$$\text{where} \quad x = \sqrt{\lambda(r^2 - 1)} \quad (41)$$

$$p_{10} = \frac{3-\lambda}{2} \quad (42)$$

where $I_1(x)$ and $I_2(x)$ are, respectively, the first and second order modified Bessel functions of the first kind. Note that the user-tunable reaction coefficient λ for the target estimation error system appears directly in the observer gains.

D. Simulation Studies

In this section we evaluate the performance of the proposed backstepping PDE observer via simulation studies. Specifically, we apply the observer to the original SPM (includes diffusion in both electrodes). Throughout these simulations we work in the normalized (r,t) coordinates, but retain the original state realization. The model parameters used in this study originate from the genetic algorithm-based parameter identification study performed on commercial lithium-iron phosphate cells in [24]. For these parameters the characteristic diffusion times (R_s^2/D_s) are 745 sec and 0.32 sec for the anode and cathode, respectively, which supports the argument for approximating cathode diffusion as instantaneous. The target system reaction coefficient is set at $\lambda = -5$. Finally, the PDE models are implemented using the finite central difference method.

The plant and observer states are initialized at different values to demonstrate uncertainty in initial conditions. Moreover, zero mean normally distributed noise with a standard deviation of 2 mV is added to the measurement. Figure 3 portrays the evolution of the spatially distributed state estimate (left column) and estimation error (right column) over the time interval $t \in [0, 0.4]$ The top and bottom rows correspond to the anode and cathode, respectively. Indeed, the estimation error converges to the origin during this time period. Also note that cathode diffusion is nearly instantaneous for the plant since its characteristic time is over three orders of magnitude faster than the anode.

The applied input current in terms of C-rate (current normalized against charge capacity) is shown in Fig. 4(a), where positive(negative) values indicate discharge(charge). Figure 4(b) demonstrates the true and estimated bulk anode SOC, defined as a normalized volume sum:

$$\theta^-(t) = \frac{3}{c_{s,max}^-}\int_0^1 r^2 c_s^-(r,t)dr \quad (43)$$

Here we see that the estimated bulk anode SOC reaches within 1% of the true value at t = 0.205. Finally, the plant output voltage with noise and estimated voltage are shown in Fig. 4(c). At t = 0.205 the voltage error is less than 1 mV.

To further quantify the estimation error Fig. 5(a) and (b) respectively portray the state and output estimation errors as functions of time. Figure 5(a) shows the L_2 spatial norm (i.e. $\int_0^1 (c_s^-(r,t) - \hat{c}_s^-(r,t))^2 dr$) of the anode concentration

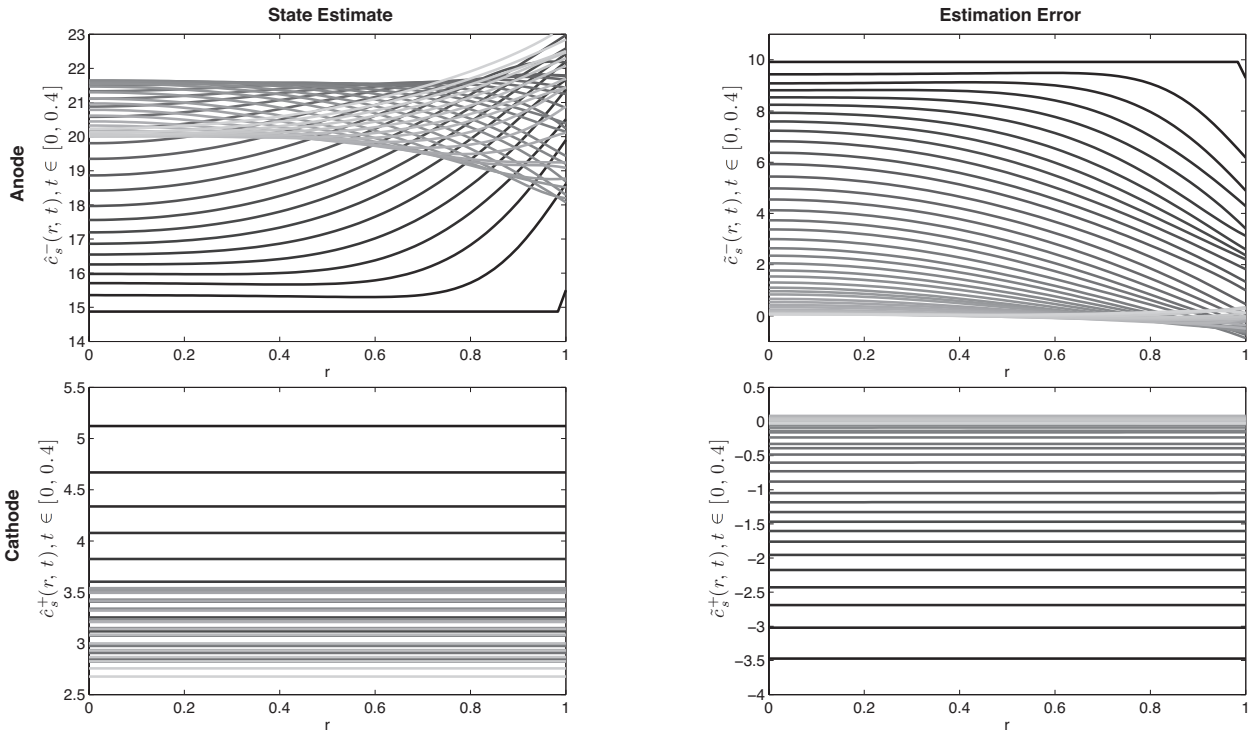

Fig. 3. Evolution of the spatially distributed state estimate and estimation error over the time interval $t \in [0, 0.4]$. As time proceeds, the curves get lighter in shade and the estimation error converges to the origin. The initial conditions are as follows. Anode: $c_s^-(r,0) = 24.8$ kmol/m^3 and $\hat{c}_s^-(r,0) = 14.9$ kmol/m^3. Cathode: $c_s^-(r,0) = 1.65$ kmol/m^3 and $\hat{c}_s^-(r,0) = 5.08$ kmol/m^3.

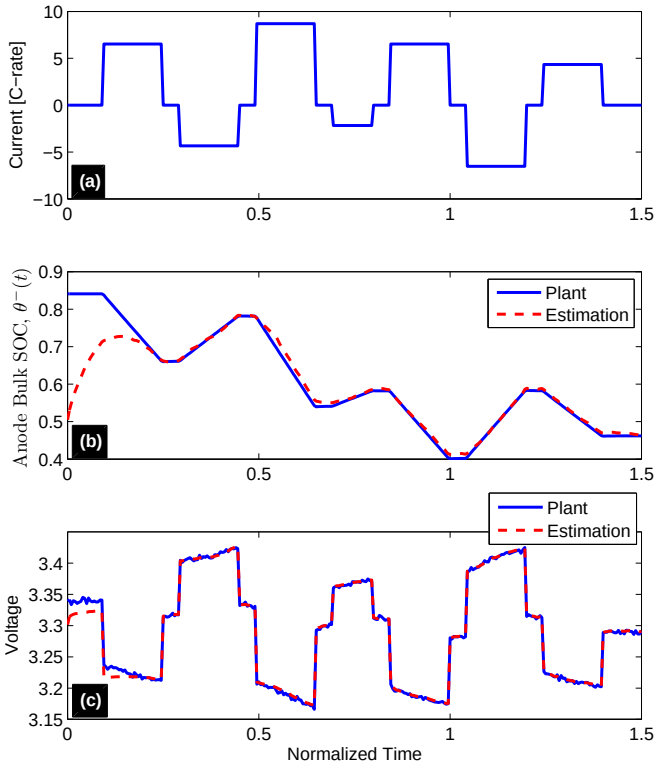

Fig. 4. (a) Input current. (b) Volume-summed bulk SOC in anode. (c) Output voltage. The measured plant voltage contains zero mean and normally distributed additive sensor noise with a standard deviation of 2 mV.

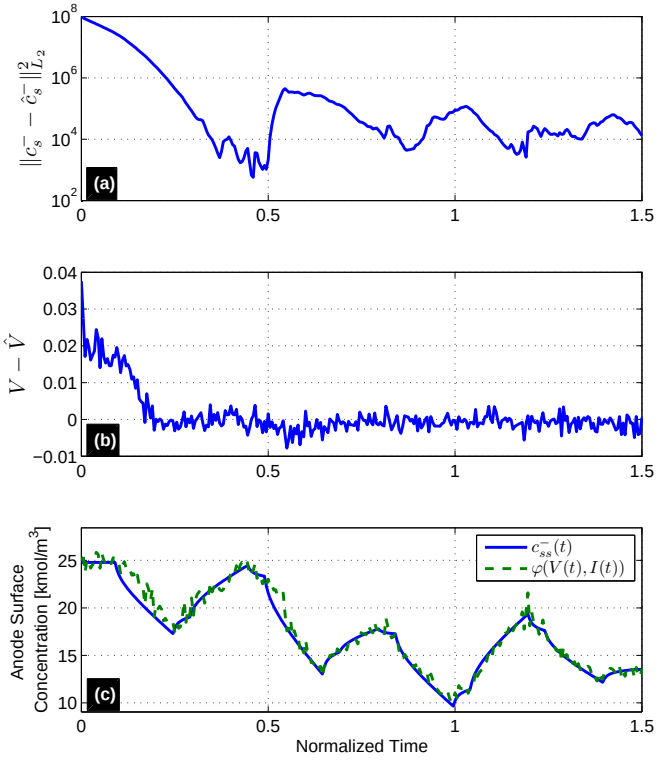

Fig. 5. Estimation Error. (a) L_2 spatial norm of anode Li concentration estimation error. (b) Voltage estimation error. (c) True anode surface concentration and processed value from inverted output function $\varphi(V(t), I(t))$.

state estimation error. Note the logarithmic scale for the vertical axis. Also shown in Fig. 5(c) is the true anode surface concentration and the processed value from the inverted output function $\varphi(V(t), I(t))$. Here we see that measurement noise and numerical inversion of the output function provide additional uncertainty into the estimator, which mathematically appears in the same manner as measurement noise. Nonetheless, the estimation error dynamics remain stable.

IV. CONCLUSION

In this paper we develop a PDE backstepping observer design for battery SOC estimation. The estimator utilizes a reduced single particle model, whose local observability properties are rigorously analyzed. The observer design process uses normalization and coordinate transformations to simplify the model's mathematical structure. Next, the PDE backstepping method is applied to derive output injection gains such that the estimation error dynamics match a linear target system whose origin is proven to be exponentially stable. Eventually we find these gains are related to the solution of a Klein-Gordon equation, which turns out to have an analytic solution. The result is a nonlinear PDE observer with a simple and elegant structure. The performance of this observer is evaluated via simulation studies.

In general battery dynamics are more complex than the single particle model utilized here. Moreover, the model parameters often degrade over time and differ across various battery materials. This motivates the development of parameter identification techniques for electrochemical battery models. This topic is the subject of the companion paper which utilizes PDE parameter identification theory developed in [26]. Moreover, we aim to analyze the composed state estimator/parameter identifier structure and evaluate its performance theoretically and experimentally.

REFERENCES

[1] N. A. Chaturvedi, R. Klein, J. Christensen, J. Ahmed, and A. Kojic, "Algorithms for advanced battery-management systems," *IEEE Control Systems Magazine*, vol. 30, no. 3, pp. 49 – 68, 2010.

[2] S. J. Moura, "Techniques for Battery Health Conscious Power Management via Electrochemical Modeling and Optimal Control," Ph.D. dissertation, University of Michigan, Ann Arbor, 2011.

[3] J. B. Siegel, X. Lin, A. G. Stefanopoulou, D. S. Hussey, D. L. Jacobson, and D. Gorsich, "Neutron imaging of lithium concentration in LFP Pouch cell battery," *Journal of the Electrochemical Society*, vol. 158, no. 5, pp. A523 – A529, 2011.

[4] M. Doyle, T. Fuller, and J. Newman, "Modeling of galvanostatic charge and discharge of the lithium/polymer/insertion cell," *Journal of the Electrochemical Society*, vol. 140, no. 6, pp. 1526 – 33, 1993.

[5] T. Fuller, M. Doyle, and J. Newman, "Simulation and optimization of the dual lithium ion insertion cell," *Journal of the Electrochemical Society*, vol. 141, no. 1, pp. 1 – 10, 1994.

[6] G. L. Plett, "Extended Kalman filtering for battery management systems of LiPB-based HEV battery packs. Part 3. State and parameter estimation," *Journal of Power Sources*, vol. 134, no. 2, pp. 277–92, 2004.

[7] ——, "Sigma-point Kalman filtering for battery management systems of LiPB-based HEV battery packs. Part 2: Simultaneous state and parameter estimation," *Journal of Power Sources*, vol. 161, no. 2, pp. 1369–1384, 2006.

[8] M. Verbrugge and E. Tate, "Adaptive state of charge algorithm for nickel metal hydride batteries including hysteresis phenomena," *Journal of Power Sources*, vol. 126, no. 1-2, pp. 236–249, 2004.

[9] M. Verbrugge, "Adaptive, multi-parameter battery state estimator with optimized time-weighting factors," *Journal of Applied Electrochemistry*, vol. 37, no. 5, pp. 605 – 616, 2007.

[10] Y. Li, D. R. Anderson, J. Song, A. M. Phillips, and X. Wang, "A Nonlinear Adaptive Observer Approach for State of Charge Estimation of Lithium-ion Batteries," in *2011 American Control Confernece (ACC)*, San Francisco, CA, United States, 2011.

[11] D. V. Do, C. Forgez, K. El Kadri Benkara, and G. Friedrich, "Impedance observer for a Li-ion battery using Kalman filter," *IEEE Transactions on Vehicular Technology*, vol. 58, no. 8, pp. 3930 – 3937, 2009.

[12] S. Santhanagopalan and R. E. White, "Online estimation of the state of charge of a lithium ion cell," *Journal of Power Sources*, vol. 161, no. 2, pp. 1346 – 1355, 2006.

[13] ——, "State of charge estimation using an unscented filter for high power lithium ion cells," *International Journal of Energy Research*, vol. 34, no. 2, pp. 152 – 163, 2010.

[14] D. D. Domenico, A. Stefanopoulou, and G. Fiengo, "Lithium-Ion Battery State of Charge and Critical Surface Charge Estimation Using an Electrochemical Model-Based Extended Kalman Filter," *Journal of Dynamic Systems, Measurement, and Control*, vol. 132, no. 6, p. 061302, 2010.

[15] K. A. Smith, C. D. Rahn, and C.-Y. Wang, "Model-based electrochemical estimation of lithium-ion batteries," in *2008 IEEE International Conference on Control Applications*, 3-5 Sept. 2008 2008, pp. 714–19.

[16] ——, "Model-based electrochemical estimation and constraint management for pulse operation of lithium ion batteries," *IEEE Transactions on Control Systems Technology*, vol. 18, no. 3, pp. 654 – 663, 2010.

[17] R. Klein, N. A. Chaturvedi, J. Christensen, J. Ahmed, R. Findeisen, and A. Kojic, "Electrochemical Model Based Observer Design for a Lithium-Ion Battery," *IEEE Transactions on Control Systems Technology*, 2012.

[18] S. Santhanagopalan, Q. Guo, P. Ramadass, and R. E. White, "Review of models for predicting the cycling performance of lithium ion batteries," *Journal of Power Sources*, vol. 156, no. 2, pp. 620 – 628, 2006.

[19] K. Thomas, J. Newman, and R. Darling, *Advances in Lithium-Ion Batteries*. New York, NY USA: Kluwer Academic/Plenum Publishers, 2002, ch. Mathematical modeling of lithium batteries, pp. 345–392.

[20] C. Chen, *Linear System Theory and Design*. Oxford University Press, Inc., 1998.

[21] M. Krstic and A. Smyshlyaev, *Boundary Control of PDEs: A Course on Backstepping Designs*. Philadelphia, PA: Society for Industrial and Applied Mathematics, 2008.

[22] C. Delacourt, P. Poizot, S. Levasseur, and C. Masquelier, "Size effects on carbon-free lifepo4 powders," *Electrochemical and Solid-State Letters*, vol. 9, no. 7, p. A352, 2006.

[23] G. Derrien, J. Hassoun, S. Panero, and B. Scrosati, "Nanostructured Sn-C composite as an advanced anode material in high-performance lithium-ion batteries," *Advanced Materials*, vol. 19, no. 17, p. 2336, 2007.

[24] J. C. Forman, S. J. Moura, J. L. Stein, and H. K. Fathy, "Parameter Identification of the Doyle-Fuller-Newman Model Based on Experimental Cycling of a Li-ion LiFePO4 Battery Using a Genetic Algorithm," *2011 American Control Conference*, 2011.

[25] H. K. Khalil, *Nonlinear Systems*, 3rd ed. Prentice Hall, 2002.

[26] M. Krstic and A. Smyshlyaev, "Adaptive control of PDEs," *Annual Reviews in Control*, vol. 32, no. 2, pp. 149–60, 12 2008.